Reduced-order model for near-wall dynamics with implications for wall models

By T. Sayadi† ‡ AND P.J. Schmid‡

The near-wall resolution requirements of wall-resolved large-eddy simulations (LES) are almost as high as those of direct numerical simulations (DNS). This restriction severely limits the applicability of LES in high-Reynolds-number flows and complex geometries that are typical of engineering configurations. An alternative to the wall-resolved LES is the wall modeled simulation, where the resolution requirement is relaxed by prescribing wall-stresses in the vicinity of walls. One such way of providing accurate values of wall-stresses is based on optimal flow-control techniques. In this study, we propose models to extend the terminology of predictive control-based wall models to complex geometries, by defining transfer functions relating the mean velocity to the second moments of coherent structures at an optimal planar location. As a result, the added calculation in the near-wall region (for example RANS) will be omitted and replaced by boundary conditions described by pre-computed transfer functions. These transfer functions are extracted using a data-driven as well as a model-based approach.

1. Background and motivation

The near-wall resolution requirements of wall-resolved LES are nearly as high as those of equivalent direct numerical simulations (DNS). This restriction severely limits the applicability of LES to high-Reynolds-number flows and complex geometries that are typical in applications of engineering interest. An alternative to the wall-resolved LES is the wall modeled simulation, where the resolution requirement is relaxed by the use of models in the vicinity of walls.

One type of wall model uses a simplified version of the turbulent boundary layer equations (TBLE) to determine the wall stress. Many different variations of these equations have been used in wall modeling. However, all of them involve solving the TBLE near the wall and using the wall stress they predict as the LES boundary condition. One example of such a model was constructed by Bodart & Larsson (2011) who neglected convection terms and integrated the equations in the wall-normal direction. The previous approaches have shown success in certain regimes, but have not demonstrated sufficient robustness in complex flows at very high Reynolds numbers. This is likely due to the fact that standard wall models rely on compensating for the missing physics of the coarse grid simulations without addressing the errors introduced through the use of subgrid scale (SGS) models or the choice of the numerical scheme. Since such errors are not known in advance, optimal flow control techniques provide alternative methods for prescribing wall stresses.

An attempt to develop such a technique was made by Nicoud *et al.* (2001), where optimal control theory was used to determine which stresses would lead to an accurate

† Aerospace Engineering Department, University of Illinois, Urbana-Champaign
‡ Department of Mathematics, Imperial College London, UK

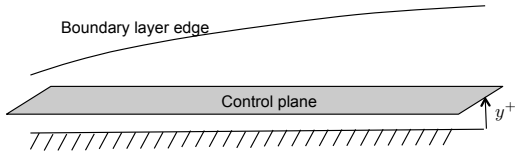

FIGURE 1: Schematic of the location of the sensing-and-control plane.

prediction of the mean velocity profile. While the results of Nicoud *et al.* (2001) illustrated the potential of control-based wall modeling, several outstanding issues remained. Using the optimal control formulation, the fluctuations were overpredicted, particularly in the streamwise velocity near the wall. To account for this, Baggett *et al.* (2000) added targets to the cost functional to regulate the velocity fluctuations; furthermore, transpiration velocity was included in the control set. This improved the prediction of the fluctuations somewhat, but rendered the mean velocity profile less accurate. Baggett *et al.* (2000) also showed that changing the finite difference scheme and using wall-normal grid stretching produced less accurate predictions of the mean velocity and, employing a different SGS model, significantly affected the accuracy — indicating that this approach would have to be re-derived for each new simulation in order to guarantee accurate results.

Templeton *et al.* (2006) improved the results of the control-based approach by incorporating the solution of the adjoint equations. The advantage of this approach was that only data near the wall was needed to define the cost functional, and the optimization procedure only solved the LES and adjoint equations in this domain. Thus, applying this technique to flows in complex geometries is more feasible since near-wall approximations can be used in defining a predictive target profile and constructing the numerical techniques used in the optimization routine. While the mean velocity profile is already known in channel flow, it is unknown in more complex geometries. Therefore, in Templeton *et al.* (2008), a Reynolds-averaged Navier-Stokes (RANS) solution is used to provide the target mean velocity information, which would alleviate this problem.

However, the averaging operation in complex geometries is less clear since there is often no homogeneous direction. The correlation coefficients demonstrate that the control only responds locally to the flow. Therefore, local averages should be used to define the cost functional. In addition, this approach relies on the RANS simulation to provide mean flow solutions. In this project, therefore, we propose models to extend the terminology of predictive control-based wall models to complex geometries, by defining transfer functions relating the mean velocity to the second moments of coherent structures at an optimal planar location, shown in Figure 1. As a result the added calculation in the near-wall region (for example RANS) will be omitted and correct boundary conditions will be described by pre-computed transfer functions. Hence, the main objective is to devise a strategy for extracting the relevant transfer functions, which are then used for this purpose.

2. Formalism

In order to determine the relation between the mean velocity and second moments of coherent structures, we employ the triple decomposition formalism of Reynolds & Hussain (1972), where a signal, f, is decomposed into a time-averaged, $\overline{f}$, phase-averaged, $\tilde{f}$, by which the background turbulence is rejected and only the organized motion is retained, and random turbulent motion, f'. We use the notation $\langle \cdot \rangle$ as the phase-averaging

operator. As a result,

$$f = \overline{f} + \tilde{f} + f', \tag{2.1}$$

with

$$\langle f \rangle = \overline{f} + \tilde{f}. \tag{2.2}$$

Some important relations resulting from this decomposition are: $\langle f' \rangle = 0$, illustrating the random nature of the background turbulence, and $\overline{\tilde{f}g'} = \langle \tilde{f}g' \rangle$, showing that the background turbulence and the organized wave motion are uncorrelated.

3. Dynamic equations for organized motion

We start with the Navier-Stokes equations for incompressible, constant-property flow, following the derivation of Reynolds & Hussain (1972),

$$\frac{\partial u_i}{\partial x_i} = 0, \tag{3.1}$$

$$\frac{\partial u_i}{\partial t} + u_j \frac{\partial u_i}{\partial x_j} = -\frac{\partial P}{\partial x_i} + \frac{1}{Re} \frac{\partial^2 u_i}{\partial x_j \partial x_j}. \tag{3.2}$$

Using the decomposition outlined in Eq. (2.1), after time- and phase-averaging the continuity equation, we obtain

$$\frac{\partial \overline{u}_i}{\partial x_i} = \frac{\partial \tilde{u}_i}{\partial x_i} = \frac{\partial u_i'}{\partial x_i} = 0 \tag{3.3}$$

Assuming steady-state solutions, phase- and time-averaging the momentum equations yields the following two equations, respectively.

$$\begin{aligned} &\frac{\partial \tilde{u}_i}{\partial t} + \overline{u}_j \frac{\partial \overline{u}_i}{\partial x_j} + \overline{u}_j \frac{\partial \tilde{u}_i}{\partial x_j} + \frac{\partial}{\partial x_j} \langle u_i' u_j' \rangle + \frac{\partial}{\partial x_j} (\tilde{u}_i \tilde{u}_j) = \\ &- \left(\frac{\partial \overline{P}}{\partial x_i} + \frac{\partial \tilde{P}}{\partial x_i} \right) + \frac{1}{Re} \left(\frac{\partial^2 \overline{u}_i}{\partial x_j \partial x_j} + \frac{\partial^2 \tilde{u}_i}{\partial x_j \partial x_j} \right) \end{aligned} \tag{3.4}$$

$$\overline{u}_j \frac{\partial \overline{u}_i}{\partial x_j} = -\frac{\partial \overline{P}}{\partial x_i} + \frac{1}{Re} \frac{\partial^2 u_i}{\partial x_j \partial x_j} - \frac{\partial}{\partial x_j} \left(\overline{u_i' u_j'} \right) - \frac{\partial}{\partial x_i} \left(\overline{\tilde{u}_i \tilde{u}_j} \right). \tag{3.5}$$

Subtracting Eq. (3.5) from Eq. (3.4) results in the dynamic equation for the coherent structures of the flow.

$$\frac{\partial \tilde{u}_i}{\partial t} + \overline{u}_j \frac{\partial \tilde{u}_i}{\partial x_j} + \tilde{u}_j \frac{\partial \overline{u}_i}{\partial x_j} = -\frac{\partial \tilde{P}}{\partial x_i} + \frac{1}{Re} \frac{\partial^2 \tilde{u}_i}{\partial x_j \partial x_j} + \frac{\partial}{\partial x_j} \left(\overline{\tilde{u}_i \tilde{u}_j} - \tilde{u}_i \tilde{u}_j \right) - \frac{\partial}{\partial x_j} \left(\langle u_i' u_j' \rangle - \overline{u_i' u_j'} \right). \tag{3.6}$$

The term $\tilde{r}_{ij} = \left(\langle u_i' u_j' \rangle - \overline{u_i' u_j'} \right)$, which appears as the last term on the right-hand side of the above equation, represents the oscillations of the background Reynolds shear stress due to the passage of the organized disturbance. In order to derive an equation for this component, we will need to first derive an equation for u_i', the turbulent component, which is obtained by subtracting Eq. (3.4) from Eq. (3.2), resulting in

$$\frac{\partial u_i'}{\partial t} + \overline{u}_j \frac{\partial u_i'}{\partial x_j} + \tilde{u}_j \frac{\partial u_i'}{\partial x_j} + u_j' \frac{\partial \overline{u}_i}{\partial x_j} + u_j' \frac{\partial \tilde{u}_i}{\partial x_j} = -\frac{\partial P'}{\partial x_i} + \frac{1}{Re} \frac{\partial^2 u_i'}{\partial x_j \partial x_j} + \frac{\partial}{\partial x_j} \left(\langle u_i' u_j' \rangle - u_i' u_j' \right). \tag{3.7}$$

The evolution equation for $u_i'u_j'$ is then obtained by multiplying Eq. (3.7) by u_i' and u_j', respectively, and adding the resulting two equations. Finally, an equation for $\tilde{r}_{ij}$ results from subtracting the phase-averaged equation for $u_i'u_j'$ from that of the time-averaged equation, which gives

$$\begin{aligned}
&\frac{\partial \tilde{r}_{ij}}{\partial t} + \overline{u}_k \frac{\partial \tilde{r}_{ij}}{\partial x_k} + \tilde{r}_{jk}\frac{\partial \overline{u}_i}{\partial x_k} + \tilde{r}_{ik}\frac{\partial \overline{u}_j}{\partial x_k} + \tilde{u}_k \frac{\partial \tilde{r}_{ij}}{\partial x_k} + \tilde{u}_k \frac{\partial \overline{u_i'u_j'}}{\partial x_k} + \overline{\tilde{u}_k \frac{\partial \tilde{r}_{ij}}{\partial x_k}} \\
&\overline{u_j'u_k'}\frac{\partial \tilde{u}_i}{\partial x_k} + \tilde{r}_{jk}\frac{\partial \tilde{u}_i}{\partial x_k} + \overline{\tilde{r}_{jk}\frac{\partial \tilde{u}_i}{\partial x_k}} \overline{u_i'u_k'}\frac{\partial \tilde{u}_j}{\partial x_k} + \tilde{r}_{ik}\frac{\partial \tilde{u}_j}{\partial x_k} + \overline{\tilde{r}_{ik}\frac{\partial \tilde{u}_j}{\partial x_k}} = \\
&\frac{\partial}{\partial x_k}(\overline{u_i'u_j'u_k'} - \langle u_i'u_j'u_k'\rangle) - \langle u_j'\frac{\partial P'}{\partial x_i}\rangle + \overline{u_j'\frac{\partial P'}{\partial x_i}} - \langle u_i'\frac{\partial P'}{\partial x_j}\rangle + \overline{u_i'\frac{\partial P'}{\partial x_j}} \\
&\frac{1}{Re}\left[\frac{\partial^2 \tilde{r}_{ij}}{\partial x_k \partial x_k} - 2\langle \frac{\partial u_i'}{\partial x_k}\frac{\partial u_j'}{\partial x_k}\rangle + 2\frac{\partial \overline{u}_i'}{\partial x_k}\frac{\partial \overline{u}_j'}{\partial x_k}\right].
\end{aligned}$$

This equation can be reformatted by keeping all linear terms on the left-hand side, and moving all nonlinear and unclosed terms, denoted as $\tilde{g}_{ij}$, to the right-hand side, leading to

$$\frac{\partial \tilde{r}_{ij}}{\partial t} + \overline{u}_k \frac{\partial \tilde{r}_{ij}}{\partial x_k} + \tilde{r}_{jk}\frac{\partial \overline{u}_i}{\partial x_k} + \tilde{r}_{ik}\frac{\partial \overline{u}_j}{\partial x_k} + \tilde{u}_k \frac{\partial \overline{u_i'u_j'}}{\partial x_k} + \overline{u_i'u_k'}\frac{\partial \tilde{u}_j}{\partial x_k} + \overline{u_i'u_k'}\frac{\partial \tilde{u}_j}{\partial x_k} - \frac{1}{Re}\frac{\partial^2 \tilde{r}_{ij}}{\partial x_k \partial x_k} = \tilde{g}_{ij}. \tag{3.8}$$

Since we are interested in the part of $\tilde{r}_{ij}$ responding to $\tilde{u}_i$, we can assume $\tilde{g}_{ij} = 0$. Knowing that the portion of $\tilde{r}_{ij}$, which responds to $\tilde{g}_{ij} = 0$, is uncorrelated from $\tilde{u}_i$, this assumption is justified.

4. Wall-bounded turbulence

In this study, we concentrate on turbulent wall-bounded flows, where the boundary layer flow assumptions apply. Therefore, the velocity component in the streamwise direction can be assumed to be relatively larger than the remaining two velocity components. In addition, the mean streamwise velocity predominately varies along the wall-normal direction, resulting in $\overline{u} = \overline{u}(y)$ and $\{\overline{v}, \overline{w}\} = 0$. Furthermore, the main contributions of the mean stresses, generated by the small scales are $\left\{\overline{u'u'}, \overline{v'v'}, \overline{w'w'}, \overline{u'v'}\right\}$, and the correlations with the spanwise component are negligible, i.e., $\left\{\overline{u'w'}, \overline{v'w'}\right\} = 0$. Finally, the derivatives in the streamwise and spanwise directions are negligible compared to the derivative in the wall-normal direction, in other words,

$$\frac{\partial}{\partial x}, \frac{\partial}{\partial z} \ll \frac{\partial}{\partial y},$$

resulting in,

$$\left\{\overline{u'u'}, \overline{v'v'}, \overline{w'w'}, \overline{u'v'}\right\} = \left\{\overline{u'u'}, \overline{v'v'}, \overline{w'w'}, \overline{u'v'}\right\}_{(y)}.$$

In order to derive the transfer functions for the organized motion, we will reformulate the equations for $\tilde{u}_i$ and $\tilde{r}_{ij}$ by Fourier transforming the variables along the homogeneous coordinate directions (x, z), as shown below

$$\{\tilde{u}_i, \tilde{r}_{ij}\}_{(x,y,z,t)} = \iint \left\{\hat{\tilde{U}}_i(t,y), \hat{\tilde{R}}_{ij}(t,y)\right\}_{(\alpha,\beta)} \exp i(\alpha x + \beta z)\, d\alpha d\beta, \tag{4.1}$$

where $\hat{\tilde{U}}_i$ and $\hat{\tilde{R}}_{ij}$ are the time-dependent eigenvectors of the adopted decomposition

for a fixed set of (α, β), and vary along the wall-normal extent of the domain. Now we can write the evolution equation for each eigenvector of the respective wave-number set (α, β). Note that for the above decomposition to be valid, the flow is assumed to be parallel in the streamwise direction. Although this assumption does not hold globally in the case of a spatially growing boundary layer, it is acceptable for a domain over which the spatial growth of the boundary layer is negligible.

4.1. *Evolution equation for* $\hat{\tilde{R}}_{ij}$

Substituting Eq. (4.1) into (3.8) and using the assumptions highlighted above, the following evolution equation for each component of (α, β) emerges

$$\frac{\partial \mathbf{R}}{\partial t} + A\mathbf{R} + B\mathbf{U} = 0, \tag{4.2}$$

where A and B are given as

$$A = \begin{bmatrix} i\alpha\overline{u} & 0 & 0 & 2\overline{u}_{,y} & 0 & 0 \\ 0 & i\alpha\overline{u} & 0 & 0 & 0 & 0 \\ 0 & 0 & i\alpha\overline{u} & 0 & 0 & 0 \\ 0 & \overline{u}_{,y} & 0 & i\alpha\overline{u} & 0 & 0 \\ 0 & 0 & 0 & 0 & i\alpha\overline{u} & \overline{u}_{,y} \\ 0 & 0 & 0 & 0 & 0 & i\alpha\overline{u} \end{bmatrix} - \frac{1}{Re}(d^2 - k^2)\mathbf{I} \tag{4.3}$$

$$B = \begin{bmatrix} 2i\alpha\overline{u'u'} + 2\overline{u'v'}d & \overline{u'u'}_{,y} & 0 \\ 0 & \overline{v'v'}_{,y} + 2i\alpha\overline{u'v'} + 2\overline{v'v'}d & 0 \\ 0 & \overline{w'w'}_{,y} & 2i\beta\overline{w'w'} \\ +i\alpha\overline{u'v'} + \overline{v'v'}d & \overline{u'v'}_{,y} + i\alpha\overline{u'u'} + \overline{u'v'}d & 0 \\ i\beta\overline{w'w'} & 0 & i\alpha\overline{u'u'} + \overline{u'v'}d \\ 0 & i\beta\overline{w'w'} & i\alpha\overline{u'v'} + \overline{v'v'}d \end{bmatrix} \tag{4.4}$$

with

$$\mathbf{R} = \begin{bmatrix} \hat{\tilde{R}}_{11} \\ \hat{\tilde{R}}_{22} \\ \hat{\tilde{R}}_{33} \\ \hat{\tilde{R}}_{12} \\ \hat{\tilde{R}}_{13} \\ \hat{\tilde{R}}_{23} \end{bmatrix} \text{ and } \mathbf{U} = \begin{bmatrix} \hat{\tilde{U}} \\ \hat{\tilde{V}} \\ \hat{\tilde{W}} \end{bmatrix}, \tag{4.5}$$

where $()_y = \partial()/\partial y$, $d = \partial/\partial y$, $k^2 = \alpha^2 + \beta^2$, and $\mathbf{I}$ denotes the identity matrix.

4.2. *Evolution equation for* $\hat{\tilde{U}}_i$

In order to derive an evolution equation for $\hat{\tilde{U}}_i$ in Fourier-space, we first rearrange Eq. (3.6) such that

$$\frac{\partial \tilde{u}_i}{\partial t} + \overline{u}_j \frac{\partial \tilde{u}_i}{\partial x_j} + \tilde{u}_j \frac{\partial \overline{u}_i}{\partial x_j} - \frac{1}{Re}\frac{\partial^2 \tilde{u}_i}{\partial x_j \partial x_j} + \frac{\partial \tilde{r}_{ij}}{\partial x_j} = \tilde{f}_i. \tag{4.6}$$

In the above expression, the coherent part of the pressure gradient and $\partial(\widetilde{\overline{u}_i\overline{u}_j} - \tilde{u}_i\tilde{u}_j)/\partial x_j$, are represented by $\tilde{f}_i$. Taking the decomposition in Fourier space as shown in Eq. (4.1)

and applying the boundary layer flow assumptions, we obtain

$$\frac{\partial \mathbf{U}}{\partial t} + C\mathbf{U} + D\mathbf{R} = \mathbf{F}, \tag{4.7}$$

where

$$C = \begin{bmatrix} i\alpha\overline{u} + \gamma & d & \\ 0 & i\alpha\overline{u} + \gamma & 0 \\ 0 & 0 & i\alpha\overline{u} + \gamma \end{bmatrix}, D = \begin{bmatrix} i\alpha & 0 & 0 & d & i\beta & 0 \\ 0 & d & 0 & i\alpha & 0 & i\beta \\ 0 & 0 & i\beta & 0 & i\alpha & d. \end{bmatrix} \tag{4.8}$$

and $\gamma = Re^{-1}(\alpha^2 + \beta^2 - d_y^2)$.

5. Extracting the coherence from the DNS data

Simulations of Sayadi *et al.* (2013) are used to extract the structures close to the wall in a turbulent boundary layer setting. In the context of the triple decomposition, coherence is the phase-averaged portion of a signal. Practically, however, phase-averaging requires many snapshots to avoid spectral leakage arising from the sample frequency, whereas the dynamic mode decomposition (DMD Schmid (2010)) is able to extract the same information from a limited number of snapshots in a robust way. Therefore, the contribution of each dynamic mode to the Reynolds shear stress can be viewed as the contribution of coherent motion from a specific phase-averaged structure.

DMD is applied to the velocity components of the flow inside the turbulent section at $Re_\theta = 1300$. Two hundred snapshots are used in the snapshot matrix. The wall-normal axis extends up to $y^+ = 140$. The DMD spectrum is shown in Figure 2. Two low-frequency modes are selected here and are highlighted in the figure. The amplitudes of these modes are identified by optimizing over the full set of sampled data using a sparsity promoting algorithm (Jovanovic *et al.* 2014).

The contribution of the coherent structures from these low-frequency modes to the components of the shear stress is shown in Figure 3. Using the triple decomposition, for example, for the streamwise component, we have

$$\overline{uu} - \overline{u}^2 = \overline{\tilde{u}\tilde{u}} + \overline{u'u'}. \tag{5.1}$$

The streamwise fluctuation represents the left-hand side of the above equation, and the coherence captures the first term on the right-hand side of the equation. What remains is the random part of the signal which appears in matrix $\mathbf{B}$. The above figure compares the contribution from the left-hand side of the above equation, representing the coherent motion, to that of the first term on the right-hand side. This figure illustrates that using two DMD modes of low frequency results in an acceptable representation of the coherent structures close to the wall, specifically, for $y^+ < 20$.

We will now analyze the structures that these low-frequency modes represent. Figure 4(a,b) show the structures, visualized by the streamwise velocity component, for modes 1 and 2, respectively; mode 1 signifies the lower frequency mode. As anticipated, these modes represent large and streaky structures concentrated closer to the wall. Mode 2 contains higher wave-numbers in the streamwise and spanwise directions compared to mode 1. The coherent structures represented by the combination of these two modes are given in Figure 4(c). From the slice in the $x - z$ plane, we can identify streaks with a width of $\Delta z^+ = 100$ that extend up to $y^+ \approx 20$. This is the size of vortices in the buffer layer, that are commonly reported in turbulent wall-bounded flows.

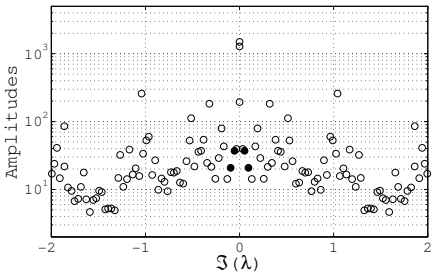

FIGURE 2: DMD spectrum. ○, all modes; ●, selected low-frequency modes.

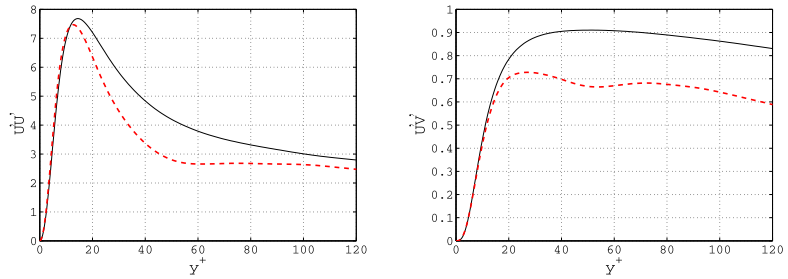

(a) Streamwise fluctuations (b) Reynolds shear stress

FIGURE 3: The contribution of the coherent structures to the fluctuating shear stresses. ——, total shear stress; − − −, contribution from mode 4 and mode 6.

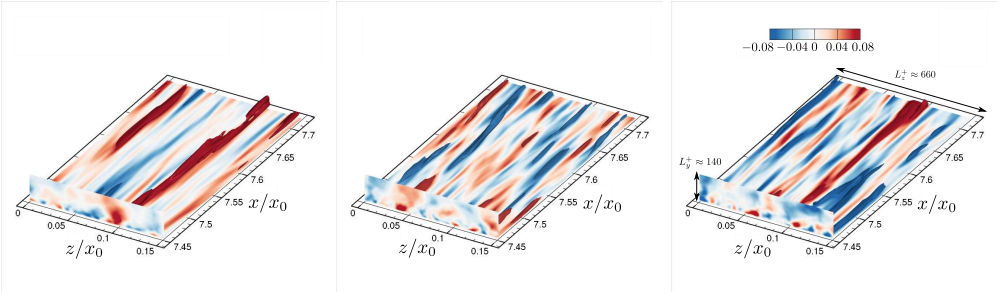

(a) Mode 1 (b) Mode 2 (c) Modes 1 & 2

FIGURE 4: Coherent structures of low frequency, visualized by the streamwise velocity component. Streamwise and spanwise directions are normalized by x_0, where $Re|_{x_0} = 10^5$.

6. Input-output analysis

Equation (4.2) constitutes a driven linearized dynamical system in state-space formulation. It is often customary to analyze this type of equation using transfer functions, derived from the assumption of a time-harmonic driving **U** leading to a time-harmonic response **R**. Due to linearity, the excitation frequency and response frequency will be identical. However, the gain, i.e., the ratio of the response amplitude to the forcing amplitude, will generally differ with frequency. The transfer function will provide infor-

mation about the filter property of the system described by (4.2): it will show which frequencies (or frequency bands) will be favored and amplified by the system and which frequencies will be damped or suppressed.

Formally, we take the Fourier transform of Eq. (4.2) which yields

$$i\omega\hat{\mathbf{R}} + A\hat{\mathbf{R}} + B\hat{\mathbf{U}} = 0; \tag{6.1}$$

where $\hat{}$ denotes now the Fourier transform of the respective variables in time. We then obtain a relation between input $\hat{\mathbf{U}}$ and output $\hat{\mathbf{R}}$ of the form

$$\hat{\mathbf{R}} = -(i\omega + A)^{-1}B\hat{\mathbf{U}}. \tag{6.2}$$

The term $(i\omega + A)^{-1}$, which is independent of the forcing, is known as the resolvent of the unforced system A which describes the inherent system dynamics in the frequency domain. The transfer function is given as $\mathsf{T} = -(i\omega + A)^{-1}B$ and its norm represents the gain in amplitude as a function of the forcing frequency. Due to our parameterization, the transfer function is also dependent on the wavenumbers in the homogeneous (streamwise and spanwise) coordinate directions; the dependence on the wall-normal direction is eliminated by discretization in this direction and by the definition of the norm. A parameter study of the transfer function (sweeping the α-β-plane) would determine the structures that are most amplified by the driving and thus should feature prominently in the flow. While this analysis gives first results on a structural selection principle, a component-wise input-output analysis could unravel more information about specific mechanisms that are responsible for an efficient transfer of energy from the coherent first-order moments $\hat{\mathbf{U}}$ to the coherent second-order moments $\hat{\mathbf{R}}$. To this end, we introduce selector-matrices P_{in} and P_{out} and modify the transfer functions as follows

$$\mathsf{T}_{\text{in}-\text{out}} = -P_{\text{out}}(i\omega + A)^{-1}BP_{\text{in}}. \tag{6.3}$$

The entries of the matrices P_{in} and P_{out} consist of zeros and ones which specify a given input, chosen among all possible inputs in $\hat{\mathbf{U}}$, and a given output, among all possible outputs of $\hat{\mathbf{R}}$. Representative of the many possible combinations, we selected P_{in} and P_{out} such as to extract the componentwise energy transfer between the streamwise coherent velocity component $\hat{\tilde{U}}$ and the coherent streamwise-velocity autocorrelation $\hat{\tilde{R}}_{11}$. This transfer has been identified in previous studies as an essential component in the energy transfer between coherent structures in near-wall turbulence. Figure 5 displays contours of the gain in the streamwise-spanwise wavenumber plane. It shows a clear preference for streamwise elongated structures, confirming experimental and numerical observations in the near-wall region. This energy transfer between $\hat{\tilde{U}}$ and $\hat{\tilde{R}}_{11}$ has to be contrasted to other forcing-response combinations which would provide insight into the most efficient energy pathways between first- and second-order moments of coherent structures and guide modeling and model-reduction efforts for the near-wall turbulence dynamics.

7. Transfer functions from subspace system identification

Besides a feature extraction approach using DMD and a componentwise input-output analysis based on an approximate model equation using a triple decomposition, we can also consider the construction of a low-dimensional model by subspace system identification. System identification is concerned with the recovery of a reduced-order model system from observed input and output data sequences. This recovery can be based on an underlying transfer function model or, as in our case, an underlying state-space model

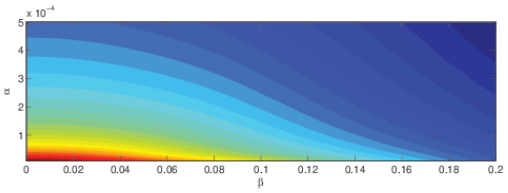

FIGURE 5: Transfer function linking coherent streamwise-velocity structures and coherent streamwise-velocity autocorrelation, visualized by contours in the streamwise-spanwise wavenumber plane.

(similar to Eq. (4.2)). Rather than formulating a time-discrete dynamical system describing a mapping over one single time-step, we repeatedly apply the dynamical system to input-output data to arrive at a formulation that links a sequence of input data to a corresponding (and time-synchronous) sequence of output data. The mapping between the two sequences involves the observability Gramian which, after proper reformulation, will yield an approximation of the system matrix A which is consistent with the observed data set. The advantage of this procedure is its robustness in producing stable low-order systems, which often poses a challenge for model-reduction efforts that involve truncation of an expansion basis. In the latter case, effects contained in the truncated structures are not reflected in the scales that are retained. In the former (system identification) case, the sum of the truncated structures are accounted for in the identified coefficients of the retained structures.

While various techniques for subspace system identification are readily available and widely applied (see, e.g., N4SID, MOESP, CVA), we will add a supplementary constraint to the identification process that promotes and enforces a low-rank final model. As the rank of a system is a discontinuous measure, taking on only integer values, which aggravates gradient-based optimization algorithms, we replace the rank of a system by its nuclear norm, defined as the sum of its singular values, and thus introduce a continuously varying measure to optimize by standard algorithms. Mathematically, the optimization problem reads

$$\text{minimize} \quad \|\mathsf{Y}\mathsf{U}^{\perp}\|_* + \gamma\|y(t) - y_{meas}(t)\|_2^2 \tag{7.1}$$

with Y and U as Hankel matrices of the output (in our case, the second-order moments) and input (in our case, the first-order moments) variables, $^{\perp}$ indicating a projection onto the null-space of U and $\|\cdot\|_*$ denoting the nuclear norm. The user-specified parameter γ balances a match between the true and model-produced measurements and the rank of the recovered model. This optimization problem can be solved using interior-point techniques, such as those given in Liu & Vandenberghe (2010). Results are forthcoming on this aspect of the project and will be reported in a future publication.

8. Conclusions

The near-wall dynamics of a turbulent boundary layer have been studied in an attempt to extract a low-dimensional system that could serve as a wall model for Large-Eddy simulations. To this end, three approaches have been taken. Dynamic mode decomposition has been applied to a sequence of snapshots and structures have been isolated by a sparsity-promoting algorithm (Jovanovic *et al.* 2014) that accurately reproduce the

Reynolds shear stress behavior near the wall. These structures show the typical elongated features readily observed in experiments and simulations. A second approach is based on a triple decomposition of the turbulent flow fields, coupled with appropriate approximations. The resulting dynamical system, linking second-order moments of the coherent structures to the first-order moments of the same structure has been formulated in a state-space representation. A transfer function analysis confirmed the dominance of streaky structures near the wall as the principal means of energy transfer. A third approach uses subspace identification techniques to extract a dynamical system not from a model equation, but rather directly from observed data. An additional side constraint enforcing low rank has been included to ensure robustness of the identified system.

Acknowledgments

We wish to acknowledge many stimulating discussions with Profs. Karthik Duraisamy, Beverley McKeon, and Mihailo Jovanovic.

REFERENCES

Baggett, J. S., Nicoud, F., Mohammadi, B., Bewley, T., Gullbrand, J. & Botella, O. 2000 Sub-optimal control based wall models for LES - including transpiration velocity. *Proceedings of the Summer Program,* Center for Turbulence Research, Stanford University, pp. 341–352.

Bodart, J. & Larsson, J. 2011 Wall-modeled large eddy simulation in complex geometries with application to high-lift devices. *Annual Research Briefs,* Center for Turbulence Research, Stanford University, pp. 37–48.

Jovanovic, M., Schmid, P. & Nichols, J. 2014 Sparsity-promoting dynamic mode decomposition. *Phys. Fluids* **26**, 024103.

Liu, Z. & Vandenberghe, L. 2010 Interior-point method for nuclear norm approximation with application to system identification. *SIAM J. Matrix Anal. Appl.* **31**, 1235–1256.

Nicoud, F., Baggett, J. S., Moin, P. & Cabot, W. 2001 Large eddy simulation wall-modeling based on suboptimal control theory and linear stochastic estimation. *Phys. Fluids* **13**, 2968.

Reynolds, W. C. & Hussain, A. K. M. F. 1972 The mechanics of an organized wave in turbulent shear flow. part 3. theoretical models and comparisons with experiments. *J Fluid Mech.* **54**, 263–288.

Sayadi, T., Hamman, C. W. & Moin, P. 2013 Direct simulation of complete H-type and K-type transitions with implications for the structure of turbulent boundary layers. *J. Fluid Mech.* **724**, 480–509.

Schmid, P. J. 2010 Dynamic mode decomposition of numerical and experimental data. *J. Fluid Mech.* **656**, 5–28.

Templeton, J. A., Wang, M. & Moin, P. 2006 An efficient wall model for large-eddy simulation based on optimal control theory. *Phys. Fluids* **18**, 025101.

Templeton, J. A., Wang, M. & Moin, P. 2008 A predictive wall model for large-eddy simulation based on optimal control techniques. *Phys. Fluids* **20**, 065104.